1521-009X/50/8/1053–1063$35.00
DRUG METABOLISM AND DISPOSITION

dx.doi.org/10.1124/dmd.121.000784
Drug Metab Dispos 50:1053–1063, August 2022

Application of Empirical Scalars To Enable Early Prediction of Human Hepatic Clearance Using In Vitro-In Vivo Extrapolation in Drug Discovery: An Evaluation of 173 Drugs[S]

Robert S. Jones, Christian Leung, Jae H. Chang, Suzanne Brown, Ning Liu, Zhengyin Yan, Jane R. Kenny, and Fabio Broccatelli

Drug Metabolism and Pharmacokinetics, Genentech, Inc., South San Francisco, California (R.S.J., C.L., Z.Y., J.R.K., F.B.); Exelixis, Drug Discovery Sciences, Alameda, California (J.H.C.); Ultragenyx Pharmaceutical Inc., Novato, California (S.B.); and Avirmax, Inc., Hayward, California (N.L.)

Received November 16, 2021; accepted May 12, 2022

ABSTRACT

The utilization of in vitro data to predict drug pharmacokinetics (PK) in vivo has been a consistent practice in early drug discovery for decades. However, its success is hampered by mispredictions attributed to uncharacterized biological phenomena/experimental artifacts. Predicted drug clearance (CL) from experimental data (i.e., intrinsic clearance: CL_{int}; fraction unbound in plasma: $f_{u,p}$) is often systematically underpredicted using the well-stirred model (WSM). The objective of this study was to evaluate using empirical scalars in the WSM to correct for CL mispredictions. Drugs ($N = 28$) were used to generate numerical scalars on CL_{int} (α) and $f_{u,p}$ (β) to minimize the absolute average fold error (AAFE) for CL predictions. These scalars were validated using an additional dataset ($N = 28$ drugs) and applied to a nonredundant AstraZeneca (AZ) dataset available in the literature ($N = 117$ drugs) for a total of 173 compounds. CL predictions using the WSM were improved for most compounds using an α value of 3.66 (~64% < 2-fold) compared with no scaling (~46% < 2-fold). Similarly, using a β value of 0.55 or combination of α and β scalars (values of 1.74 and 0.66, respectively) resulted in a similar improvement in predictions (~64% < 2-fold and ~65% < 2-fold, respectively). For highly bound compounds ($f_{u,p} \leq 0.01$), AAFE was substantially reduced across all scaling methods. Using the β scalar alone or a combination of α and β appeared optimal and produced larger magnitude corrections for highly bound compounds. Some drugs are still disproportionally mispredicted; however, the improvements in prediction error and simplicity of applying these scalars suggest its utility for early-stage CL predictions.

SIGNIFICANCE STATEMENT

In early drug discovery, prediction of human clearance using in vitro experimental data plays an essential role in triaging compounds prior to in vivo studies. These predictions have been systematically underestimated. Here we introduce empirical scalars calibrated on the extent of plasma protein binding that appear to improve clearance predictions across multiple datasets. This approach can be used in early phases of drug discovery prior to the availability of preclinical data for early quantitative predictions of human clearance.

Introduction

The utilization of in vitro data to predict in vivo pharmacokinetic parameters is widely adopted, and many groups have evaluated and developed approaches to predict in vivo clearance. These approaches use in vitro data such as intrinsic clearance (CL_{int}), free fraction of drug in plasma ($f_{u,p}$), and nonspecific binding in the in vitro matrices ($f_{u,inc}$), as well as measures of drug properties such as lipophilicity ($log_{D,pH=7.4}$) and ionization class (anionic, basic, neutral, or zwitterion) (Hallifax et al., 2010). Attempts to use these data to improve in vitro-in vivo extrapolation (IVIVE) through different scaling approaches have yielded varying degrees of success (Grime and Riley, 2006; Berezhkovskiy, 2011; Ring et al., 2011; Hallifax and Houston, 2012). Recently, researchers have expanded on these approaches to assess prediction accuracy and have evaluated the advantages and disadvantages among the various methods (Lombardo et al., 2014, 2018; Benet and Sodhi, 2020; Umehara et al., 2020; Poulin and Haddad, 2021).

Among the physiologically relevant liver models for CL predictions, the well-stirred model (WSM) is broadly adopted (Pang and Rowland, 1977a,b). The perquisite of the WSM is that the rate of enzyme-mediated elimination is slower compared with both the rate of distribution and kinetics of plasma protein binding and assumes that the unbound drug concentration in plasma and in the hepatic aqueous environment reach instantaneous equilibrium and undergo linear kinetics.

All of the authors were employees at Genentech at the time that they contributed to the manuscript. This work received no external funding.

The authors declare that they have no conflicts of interest with the contents of this article.

dx.doi.org/10.1124/dmd.121.000784.

[S] This article has supplemental material available at dmd.aspetjournals.org.

ABBREVIATIONS: AAFE, absolute average fold error; AFE, average fold error; AZ, AstraZeneca; BPP, blood to plasma partitioning; CL, clearance; CL_{hep}, hepatic plasma clearance; CL_{int}, intrinsic clearance; CL_{obs}, observed human plasma clearance; CL_{pred}, predicted human plasma clearance; CYP450, cytochrome P450; FDA, US Food and Drug Administration; $f_{u,inc}$, fraction unbound in incubation; $f_{u,mic}$, fraction unbound in microsomes; $f_{u,p}$, fraction unbound in plasma; $f_{u,p,adjusted}$, adjusted fraction unbound in plasma; GNE, Genentech; HPLC, high-performance liquid chromatography; IS, internal standard; IVIVE, in vitro-in vivo extrapolation; LC-MS/MS, liquid chromatography–tandem mass spectrometry; LM, liver microsome; $log_{D,pH=7.4}$, lipophilicity; PK, pharmacokinetics; R^2, coefficient of determination; RED, rapid equilibrium dialysis; $t_{1/2}$, half-life; WSM, well-stirred model.

In its simplest form, the WSM can be expressed as:

$$CL_{hep,b} = \frac{Q_{hep} \cdot CL_{int}}{Q_{hep} + CL_{int}} \quad (1)$$

in which $CL_{hep,b}$ is the hepatic blood CL, Q_{hep} is the hepatic blood flow, and CL_{int} is the intrinsic clearance of the blood perfused liver.

When assuming that the concentration in blood cells is comparable to plasma, $CL_{hep,b}$ equates to hepatic plasma clearance (CL_{hep}). Furthermore, as only the free drug is assumed to be metabolized, the equation can be rearranged as:

$$CL_{hep} = \frac{Q_{hep} \cdot f_{u,p} \cdot CL_{int,u}}{(Q_{hep} + f_{u,p} \cdot CL_{int,u})} \quad (2)$$

in which CL_{hep} is the hepatic plasma clearance, $f_{u,p}$ is the fraction unbound in plasma, and $CL_{int,u}$ is the intrinsic clearance of the free drug.

"Bottom-up" approaches to CL_{hep} prediction aim to describe $CL_{int,u}$, starting from in vitro measurements in systems such as liver microsomes or hepatocytes and correcting for unbound fraction. Although this approach is useful, its quantitative accuracy is still somewhat limited and the underlying mechanisms responsible for the systematically observed underpredictions are not fully understood. Although there is a lack of consensus as to the identity and magnitude of each reason leading to poor CL predictions, the tendency to often underpredict CL_{int} could be rationalized as a loss of activity in the hepatocyte cultures compared with in vivo systems or by imprecise estimation of the appropriate physiologic scalars (Bowman and Benet, 2019). These possibilities suggest that a constant CL_{int} multiplier could be derived to improve in vitro-in vivo correlations. This practical approach was shown to considerably improve IVIVE by AstraZeneca (Williamson et al., 2020). Internally at Genentech, we have observed a similar degree of improvement for clinical and preclinical predictions using the same approach; disappointingly, we have observed that in vitro estimates of in vivo CL_{int} were still suboptimal for highly bound compounds (also witnessed in the AstraZeneca dataset).

Many recent reports have emphasized a potential role of plasma proteins in hepatic drug uptake, producing an abundance of in vivo and in vitro data supporting the notion that hepatic uptake and ultimately CL_{hep} increase with increasing binding to plasma proteins, specifically albumin (Poulin and Haddad, 2015; Bowman et al., 2019; Chang et al., 2019; Kim et al., 2019; Francis et al., 2021). In particular, Francis et al. (2021) used data collected from 26 compounds in rat and human hepatocytes to derive an empirical equation to account for the impact of plasma protein on $CL_{int,u,in\ vitro}$ in an effort to improve IVIVE-based CL predictions.

Although the mechanism of such phenomena is still unclear, this could potentially arise from a transporter-albumin interaction or could be unrelated to transporter activity. Because of the overlapping chemical space between hepatic uptake transporters and albumin substrates (i.e., lipophilic anionic compounds), finding chemical probes to investigate each hypothesis has proven challenging. The fact that plasma protein-mediated hepatic uptake is currently unaccounted for in current models of hepatic clearance may support the derivation of a CL_{int} scalar based on $f_{u,p}$ magnitude.

In this study, a trend analysis approach was used to derive two scalars, "α" for CL_{int} and "β" for $f_{u,p}$, from a training set of compounds with human intravenous PK data. Here we report the impact of including different scalars in the WSM and subsequent improvements in the prediction of human CL_{hep} for 173 compounds.

Materials and Methods

Human CL and Physiochemical Properties Dataset. The internal Genentech (GNE) dataset was generated by collecting plasma protein binding ($f_{u,p}$), fraction unbound in microsomes ($f_{u,mic}$), and in vitro intrinsic clearance (CL_{int}) parameters for 56 drugs. pKa and ionization class were calculated using the software MoKa (Molecular Discovery: https://www.moldiscovery.com/software/moka/). The base pKa model was augmented by including Roche and GNE compounds in the training set. Intravenous CL data were collected primarily from Lombardo et al. (2018) but also from the DrugBank database (https://www.drugbank.ca/). The definitions for primary route of elimination and experimental $\log_{D,pH=7.4}$ were also retrieved from various sources: Lombardo et al. (2014), DrugBank, and Benet et al. (2011). When experimental $\log_{D,pH=7.4}$ was not available, a GNE internal machine learning model was used for prediction. For compounds for which the route of elimination in human was found to be metabolic, further investigation concerning major metabolizing enzymes was performed using DrugBank; when the information was not available in DrugBank, individual searches were performed using alternative resources: Kyoto Encyclopedia of Genes and Genomes (KEGG: https://www.genome.jp/kegg/), US Food and Drug Administration (FDA: https://www.fda.gov/), and literature references (Laurenzana and Owens, 1997; Shet et al., 1997; Moridani et al., 2001; Li et al., 2002; McDonald and Rettie, 2007; Olkkola and Ahonen, 2008; He et al., 2009; Jornil et al., 2010; Yu et al., 2014; Salerno et al., 2017; MacLauchlin et al., 2018; Kogame et al., 2019). Human CL endpoints were capped to a liver blood flow value of 20.7 ml/min/kg; when mixed mechanisms of elimination were reported, the total CL was normalized according to the fraction of hepatic metabolism (moxifloxacin and zidovudine).

In addition, a total of 78 compounds for which the major route of elimination in humans is mediated by cytochrome P450 (CYP450; $N = 51$), phase II metabolism ($N = 9$), renal elimination ($N = 15$), or biliary elimination ($N = 3$) were included in a separate dataset to explore the relationship between elimination route and physiochemical properties. For six nonmetabolically eliminated compounds for which experimental $f_{u,mic}$ was lacking, values were predicted using GNE's in-house internal machine learning model. Four of the 60 metabolically eliminated compounds are not in the final dataset due to significant extra hepatic elimination (zidovudine, moxifloxacin), nonlinear pharmacokinetics (tacrine), and significant disconnects between the plasma protein binding value reported in literature compared with the ones reported in house (Gammans et al., 1986; Madden et al., 1995; Moise et al., 2000).

External Validation Set. The data presented in the recent publication from AstraZeneca (AZ) scientists were used as an external validation set (Williamson et al., 2020). Compounds were included if the human CL value could be retrieved from Lombardo et al. (2018). Compounds that were already present in the GNE dataset were excluded to avoid duplication. It is important to highlight that in the AZ dataset, $CL_{int,u}$ of the free drug in hepatocytes is provided as a single value and not as a combination of apparent CL_{int} and $f_{u,mic}$, whereas in the GNE dataset, all of the $f_{u,mic}$ values for metabolically eliminated compounds are experimentally determined and presented separately.

Materials. The 56 compounds in the GNE dataset were obtained from commercial sources (Sigma-Aldrich, Cayman Chemical, Toronto Research Chemicals, etc.) via the internal compound management bank. Compounds were prepared as 10 mM or 1 mM stock concentrations in dimethyl sulfoxide (DMSO). Pooled male and female human ($N = 10$) hepatocytes were purchased from BioIVT (Westbury, NY); high-performance liquid chromatography (HPLC)-grade water was from J.T. Baker (Center Valley, PA); HPLC-grade acetonitrile was from EMD Millipore (Billerica, MA). Dulbecco's Modified Eagle Medium (DMEM) and rapid equilibrium dialysis (RED) devices with inserts were obtained from Thermo Fisher Scientific Inc. (Rockford, IL). Pooled ($N \geq 10$) male and female human liver microsomes were purchased from Corning (Woburn, MA). An Allegra × 12R centrifuge used in these studies was purchased from Beckman Coulter (Brea, CA). All other chemicals and reagents were of analytical grade and were obtained from Sigma-Aldrich (St. Louis, MO) unless otherwise specified.

Hepatocyte Stability. Metabolic hepatocyte stability was determined in house using cryopreserved primary hepatocytes. Drug and hepatocyte dilutions were performed in DMEM with 1 μM drug concentration (final DMSO concentration 0.1% v/v) and 0.5 million cells ml^{-1} under 37°C with 5% CO_2. A master reaction plate containing drug and hepatocyte reaction mixture was prepared and aliquots were removed and quenched with acetonitrile and internal standard (IS)

at 0, 1, 2, and 3 hours. The samples were centrifuged at 3700 rpm for 15 minutes, and the supernatant was diluted equally with water before liquid chromatography–tandem mass spectrometry (LC-MS/MS) analysis. If irregular time course was observed using the above protocol (e.g., increase in drug concentration or variability over time), a follow-up experiment was performed using a different quench/crash protocol where individual, total reactions were crashed for each time point (crash-in) (Winiwarter et al., 2019) using quadruplicate reaction plates containing the drug and hepatocyte mixture. Out of the 18 compounds for which both protocols were available, only two produced qualitatively different results (>3-fold change). These discrepancies were attributed to the high degree of nonspecific binding to the incubation plate, which resulted in high variability or increase in analyte concentrations over time, which was diminished upon using the crash-in method. Acetonitrile with IS was added to the separate reaction mixtures at 0, 1, 2, and 3 hours. The samples were centrifuged at 3700 rpm for 15 minutes, and the supernatant was diluted equally with water before LC-MS/MS analysis.

Microsomal Incubational Binding. Liver microsome (LM) binding experiments were performed in triplicate using a RED Device. LM stock solutions were diluted to 0.5 mg protein/ml with phosphate buffer saline (PBS: 133 mM potassium phosphate, 150 mM sodium chloride). Drugs were diluted to 1 μM in the LM solution. Subsequently, 500 μl of PBS was added to the receiver wells of the RED device and 300 μl of the drug-LM mixtures was added to the donor wells of the RED device. The RED device was sealed using a gas-permeable membrane and then placed in a shaking incubator (450 rpm; VWR Symphony) at 37°C with 5% CO_2. After 6 hours, aliquots from the receiver and donor wells of the RED device were added to acetonitrile with IS and matrix equalized. The samples were centrifuged at 3700 rpm for 15 minutes, and the supernatant was diluted equally with water before LC-MS/MS analysis.

Plasma Protein Binding. Plasma protein binding experiments were performed in triplicate using a single-use RED device. Plasma was adjusted to pH 7.4 with 0.5 M phosphoric acid. Drugs were diluted to 5 μM in plasma. Five hundred microliters of PBS was added to the receiver wells of the RED device, and 300 μl of the drug-plasma mixtures was added to the donor wells of the RED device. The RED device was sealed using a gas-permeable membrane and then placed in a shaking incubator (450 rpm; VWR SymphonyTM) at 37°C with 5% CO_2. After 6 or 24 hours, buffer and plasma aliquots from the receiver and donor wells of the RED device were matrix equalized with an equal volume of plasma or buffer, and ice-cold acetonitrile was added with IS. The samples were centrifuged at 3700 rpm for 15 minutes, and the supernatant was diluted equally with water before LC-MS/MS analysis.

LC-MS/MS Analysis. LC-MS/MS analysis was performed using a 5500+ QTRAP mass spectrometer coupled with a TurboIonSpray ESI ion source (AB SCIEX, Redwood City, CA) and Agilent 1200 series LC (Santa Clara, CA). Chromatographic separation of all analytes was achieved using a Kinetex C18 column (50 × 2.0 mm, 80 Å, 4 μm particle size) (Torrance, CA) along with mobile phase A consisting of 0.1% formic acid in HPLC-grade water and mobile phase B consisting of 0.1% formic acid in acetonitrile. A generic LC gradient was used for all analytes where the flow rate was set to 0.5 ml/min, the run time to 3.5 minutes, and the LC gradient as follows: 2% B for the first 1.5 minutes, ramped up to 40% B from 1.5 to 2.0 minutes, remained constant at 98% B from 2.0 to 3.0 minutes, and then decreased to 2% B from 3.0 to 3.5 minutes.

Data Analysis. For the hepatocyte stability experiments, half-life ($t_{1/2}$) and CL_{int} were determined for each compound after calculating the slope of the natural log plot of percent parent remaining profiles over time using the mass spectrometer (MS) peak area ratios normalized to initial time point peak area (t = 0 min). $t_{1/2}$ was calculated using the following equation:

$$t_{1/2}(min) = \frac{\ln(2)}{-Slope} \tag{3}$$

CL_{int} was subsequently calculated using the scaling factors for hepatocytes to whole body intrinsic clearance (ml/min/kg):

$$CL_{int}(mL/min/kg) = \frac{\ln(2)\cdot V/P}{t_{1/2}} \cdot \frac{1\ mL}{1000\ \mu L} \cdot \frac{million\ hepatocytes}{gram\ liver} \cdot \frac{gram\ liver}{kg\ body\ weight} \tag{4}$$

V/P is defined as the incubation volume divided by the number of hepatocytes used in the incubation (μl/x 10^6 cells), million hepatocytes/gram liver is 135 × 10^6 cells/g liver, and gram liver/kg body weight is 25.7 g liver/kg body weight based on previously published literature data. For the AZ dataset, these values were originally reported as μl/min/x 10^6 cells and were scaled using the same physiologic scalars used internally for scaling human hepatocyte stability studies to calculate whole body intrinsic clearance (ml/min/kg). $CL_{int,u}$ values were calculated using reported unbound fraction in the incubation ($f_{u,inc}$) for each compound in the AZ dataset (Williamson et al., 2020).

Fraction unbound in plasma ($f_{u,p}$) and microsomes ($f_{u,mic}$) were calculated using peak area ratios between the analyte and the IS from the receiver and the donor chambers using the following equation:

$$f_u = \left(\frac{analyte\ peak\ area}{IS\ peak\ area}\right)_{receiver} \Big/ \left(\frac{analyte\ peak\ area}{IS\ peak\ area}\right)_{donor} \tag{5}$$

Derivation of Scalars for CL_{int} and $f_{u,p}$. The GNE dataset was divided into a training set (N = 28) and a validation set (N = 28) for the scalar definition. The subset sampling was performed by alternating compound assignment based on a decreasing value for their $f_{u,p}$. An AZ dataset was used as an additional validation set (N = 117 compounds).

Three approaches to offset derivation were attempted, starting from the following formula:

$$CL_{hep} = \frac{Q_{hep}\cdot CL_{int,u}\cdot \alpha \cdot {f_{u,p}}^{\beta}}{Q_{hep} + CL_{int,u}\cdot \alpha \cdot {f_{u,p}}^{\beta}} \begin{cases} \alpha > 1,\ \beta = 1\ \ Method\ 1 \\ \alpha = 1,\ \beta < 1\ \ Method\ 2 \\ \alpha > 1,\ \beta < 1\ \ Method\ 3 \end{cases} \tag{6}$$

The CL_{int} offset method 1 is used to derive the scalar α while setting the scalar β equal to 1, method 2 is used to derive the scalar β while setting the scalar α equal to 1, and lastly method 3 is used to derive both the α and β scalars simultaneously. All three methods assume that the main reasons for in vitro to in vivo disconnects are consistent across hepatic-metabolized drugs. In addition, the application of an exponential β scalar on $f_{u,p}$ could also be mathematically rearranged to yield a $f_{u,p}$-dependent scalar on the product of $CL_{int,u}\cdot f_{u,p}$ [i.e., ${f_{u,p}}^{\beta-1}\cdot(CL_{int,u}\cdot f_{u,p})$], analogous to the approach defined by Francis et al. (2021) in which $CL_{int,u}$ is scaled by a factor of plasma protein binding. A simulation between these two approaches is presented in Supplemental Fig. 3.

These assumptions ignore the potential activity of uptake transporters for practical reasons, not scientific ones. The impact of transporters on newer iterations of the WSM are discussed elsewhere (Endres et al., 2009; Pang et al., 2019). Blood to plasma partitioning (BPP) is also an important parameter within the WSM equation. In particular, BPP can greatly vary the predicted hepatic CL for high CL_{int} compounds; for compounds that exhibit low $CL_{int,u}$ and/or $f_{u,p}$, the hepatic CL predicted by the WSM can be approximated by $CL_{int,u}\cdot f_{u,p}$, and is minimally affected by the BPP value. Although it is acknowledged that in some cases the availability of BPP data could significantly improve predictions, the improved accuracy observed for high CL compounds suggests that availability of measured BPP data would not change the general conclusions from this study. Therefore, for the purpose of this analysis, BPP was assumed to be 1.

The scalars were derived using a grid search across parameter values (α ranging from 1 to 5 with a step of 0.01, β ranging from 0 to 1 with a step of 0.01). The optimal values were selected based on the minimization of average fold error (AFE) and absolute average fold error (AAFE) in the prediction of human clearance CL_{pred}; AAFE was defined as follows:

$$AFE = 10^{\frac{1}{N}\Sigma \log\left(\frac{CL_{pred}}{CL_{obs}}\right)} \tag{7}$$

$$AAFE = 10^{\frac{1}{N}\Sigma \left|\log\left(\frac{CL_{pred}}{CL_{obs}}\right)\right|} \tag{8}$$

The grid search was performed using RStudio, and the datasets are provided in the Supplemental Material. The values were derived based on the GNE training set of 28 compounds, whereas the whole GNE dataset (N = 56) and the AZ (N = 117) dataset combined (N = 173) were used to assess the generalizability of the approach.

Due to the higher number of non–highly bound compounds ($f_{u,p} > 0.01$) and due to the inherent differences between the two approaches being defined by variable binding characteristics, the analysis of data was stratified for high ($f_{u,p} \leq 0.01$) versus low/moderate binders ($f_{u,p} > 0.01$); after the validation in the external GNE set, the datasets were combined to increase the representation of highly bound compounds. The three methods were compared with the WSM with no offset scalars (α and β = 1).

Results

Properties of the Dataset. The physiochemical properties of the GNE dataset ($N = 56$) and nonredundant compounds ($N = 117$) in the AZ dataset (Williamson et al., 2020) were investigated. The full compound list and parameters used for CL predictions are available in Supplemental Tables 1 and 2. Figures 1 and 2 display the ion class, extent of plasma protein binding, and major route of elimination for the GNE and AZ datasets, respectively. The distribution of compounds across physiochemical space was relatively consistent across the two datasets. In terms of $f_{u,p}$, the GNE dataset had 11 compounds that were highly bound ($f_{u,p} \leq 0.01$) and the AZ dataset had 15 highly bound compounds ($f_{u,p} \leq 0.01$). All of the compounds in the GNE dataset were cleared primarily via phase I and II metabolic elimination (87.5% and 12.5%, respectively). Compounds in the AZ dataset were also primarily cleared via phase I (~79.5%) and phase II (~7.7%) metabolism; in addition, 15 compounds were cleared via alternative or unknown routes of elimination (~12.8%).

A summary of the reported observed human plasma clearances (CL_{obs}) is depicted in Figure 3, with medians of 4.7 ml/min/kg and 6.1 ml/min/kg for the GNE and AZ datasets, respectively. A statistical comparison between all individually reported mean observed CL values for both datasets (GNE and AZ) was performed to assess whether they were statistically different and whether there was bias for higher or lower reported CL values from each dataset. There were no statistically significant differences between the mean observed CL values for compounds used in both datasets (data not shown; two-way unpaired *t* test and Mann-Whitney test, $P > 0.05$). Supplemental Figure 1 shows the $CL_{int,u}$ corrected for microsomal binding versus the $\log_{D,pH=7.4}$ values for each compound stratified by mechanism of elimination. Incubational binding ($f_{u,inc}$) was assumed to be comparable between human LM and human hepatocytes based on previously published data (Chen et al., 2017; Winiwarter et al., 2019). Although ionization class tended to be evenly distributed across the respective range of $CL_{int,u}$ values, it was apparent that for compounds primarily undergoing CYP450-mediated elimination, there were increases in elimination rate ($CL_{int,u}$) with an increase in lipophilicity ($\log_{D,pH=7.4}$) (Benet et al., 2011; Varma et al., 2015). In the −0.5–1 $\log_{D,pH=7.4}$ range, a $CL_{int,u}$ greater than 3 ml/min/kg predicted compounds eliminated in the liver with no exception (all via hepatic metabolism, with the exception of one compound via biliary elimination), whereas in the same $\log_{D,pH=7.4}$ range, it was visually apparent that renal elimination was as likely as metabolic elimination for compounds with in vitro metabolic turnover of under 3 ml/min/kg based on this dataset (three compounds renally eliminated vs. five metabolically eliminated). Values of $\log_{D,pH=7.4} < -0.5$ identified renally eliminated compounds in all cases except for one biliary-eliminated outlier; similarly, values of $\log_{D,pH=7.4} > 1$ identified all metabolically eliminated compounds in all cases except for one biliary-eliminated outlier.

CL Predictions Using WSM Scalars. Using independent datasets from two different companies within the pharmaceutical industry, different empirical scalars were derived to correct for mispredicted compounds using the WSM for compounds with a range of physiochemical

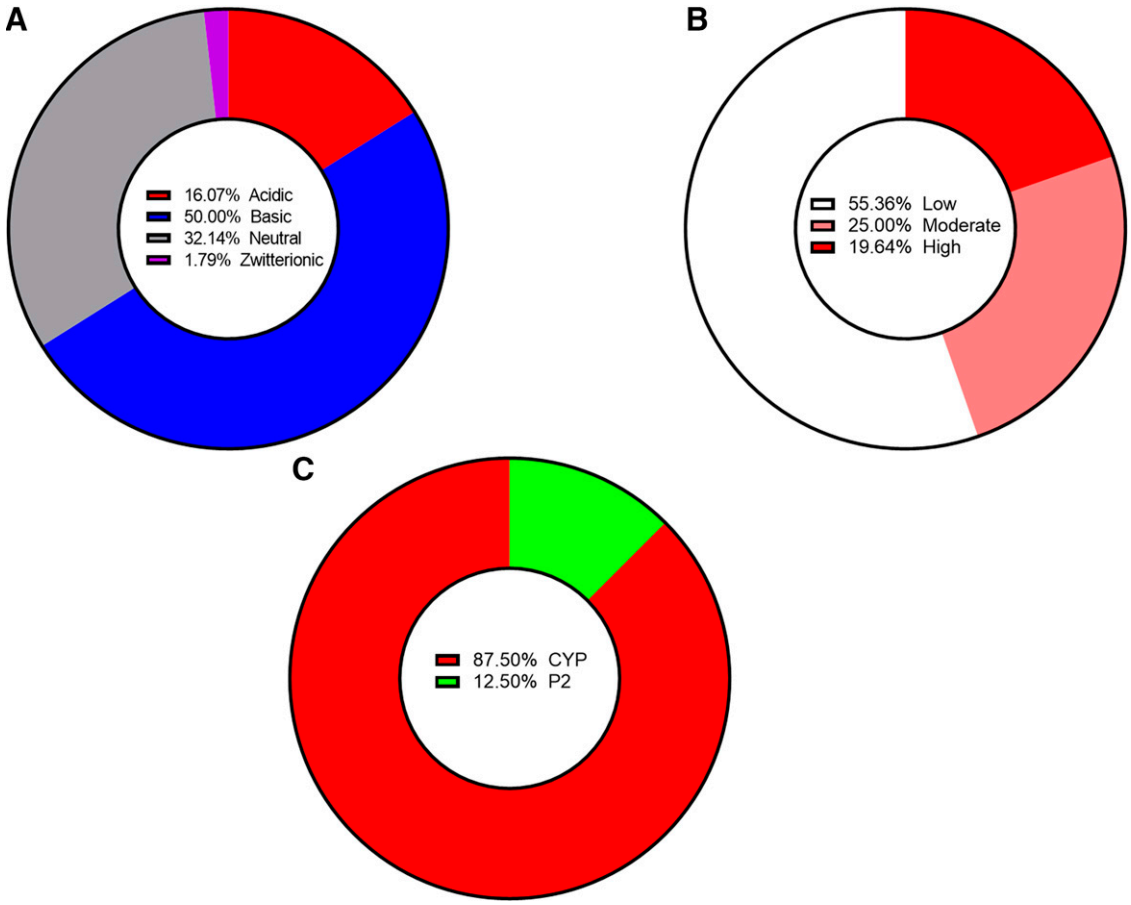

Fig. 1. Physiochemical and absorption, distribution, metabolism, and excretion (ADME) properties of the GNE dataset ($N = 56$). (A) Ion class; (B) extent of plasma protein binding (low: $f_{up} > 0.10$, moderate: $0.01 < f_{up} \leq 0.10$, high: $f_{up} \leq 0.01$); and (C) major route of elimination.

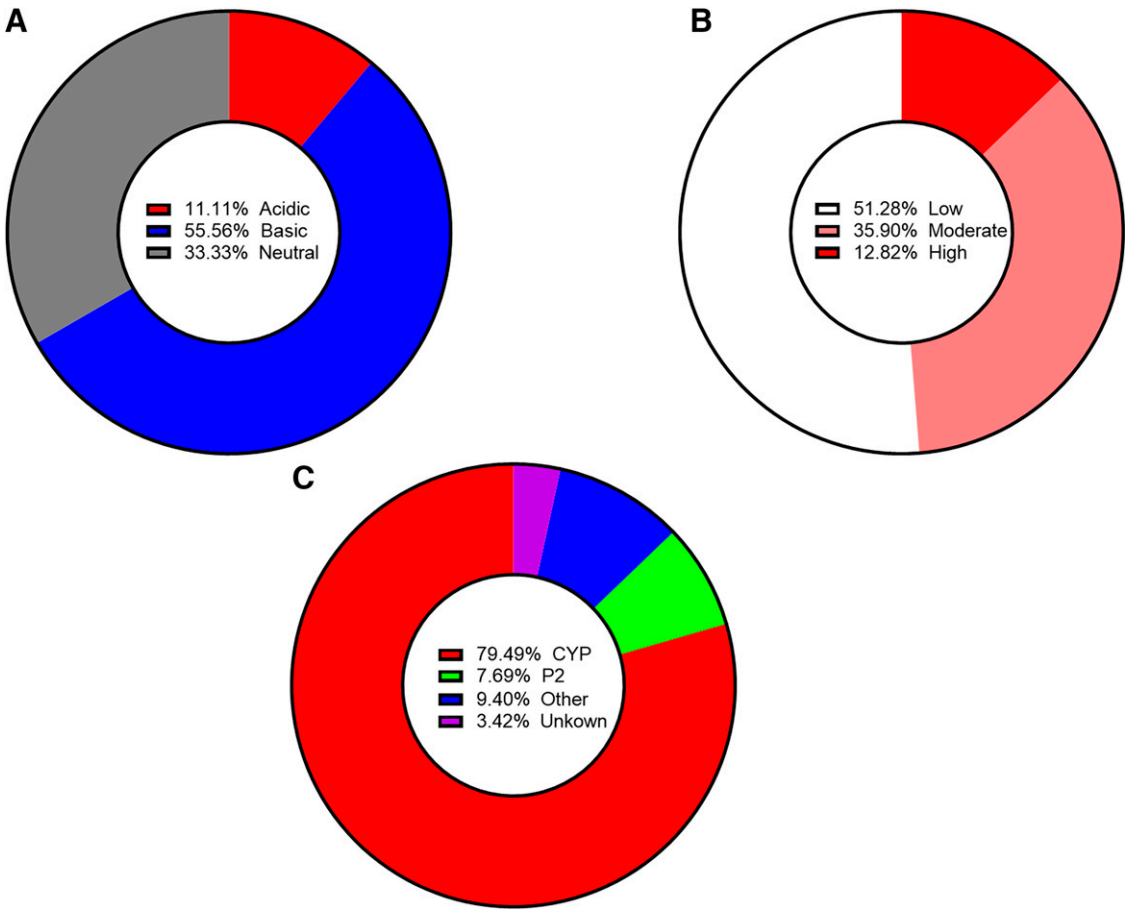

Fig. 2. Physiochemical and ADME properties of the AZ dataset (N = 117). (A) Ion class; (B) extent of plasma protein binding (low: $f_{u,p} > 0.10$, moderate: $0.01 < f_{u,p} \leq 0.10$, high: $f_{u,p} \leq 0.01$); and (C) major route of elimination.

properties. These scalars were derived using a grid search in RStudio aimed at minimizing AFE and AAFE for a set of compounds randomly selected from the GNE dataset (GNE training, N = 28). The remaining GNE compounds in the dataset (GNE validation, N = 28) were used to validate each modeling method for our internally collected data, and each modeling scheme was subsequently applied to all of the compounds for each method (GNE + AZ datasets, N = 173). Prior to fitting these scalars, each dataset was used to predict total clearance without the use of any empirical scalars by using the well-stirred model (α = 1, β = 1). Figure 4 depicts the AFE for each compound for the GNE training, GNE validation, and combined datasets with no scalars applied. The majority of compounds were underpredicted when comparing CL_{pred} to CL_{obs} for each of the three datasets. Table 1 provides a summary of the fraction of compounds that were within/beyond 2-fold AAFE and coefficients of determination (R^2) for each dataset and modeling method, and these are further stratified by degree of plasma protein binding in Table 2. Additionally, the correlation plots of CL_{pred} versus CL_{obs} of the GNE + AZ datasets for each of the scaling methods are provided in Supplemental Fig. 2. The percentage of compounds that were less than 2-fold AAFE CL_{pred} values for the GNE training, GNE validation, and GNE + AZ datasets were 32.1%, 53.6%, and 45.7%, respectively. Subsequently, using the GNE training dataset and each of the modeling methods, α and β scalar values were individually and simultaneously fitted using the approaches outlined in the methods. Figure 5 shows the different datasets after fitting the offset α scalar (method 1) and fixing β to 1. After performing the analysis, an offset α value of 3.66 was obtained to minimize the AAFE for the GNE training dataset; this was consistent with previous reports (Williamson et al., 2020). As expected, the CL_{pred} values were increased compared with the model predictions using no scalars due to the product of $\alpha \cdot CL_{int,u} \cdot f_{u,p}$, where $\alpha > 1$, which improved the prediction for a majority of the compounds that were originally underpredicted. The percentage of compounds that were less than 2-fold AAFE CL_{pred} values for the GNE training, GNE validation, and GNE + AZ datasets were substantially reduced compared with the model prediction with no scalars (60.7%, 71.4%, and 63.6%, respectively) (Table 1). Using method 2, where α was

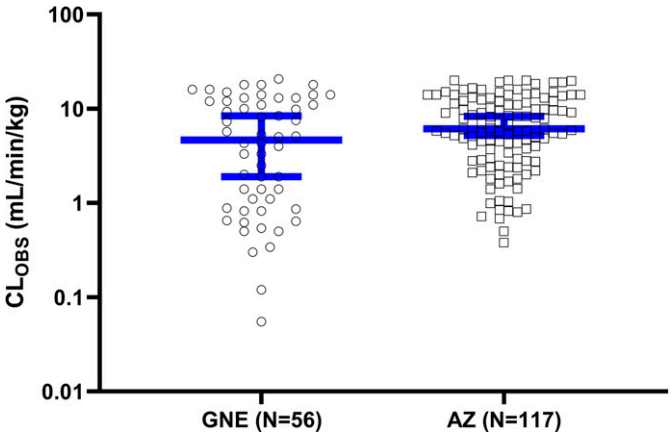

Fig. 3. Observed human plasma CL of GNE and AZ datasets. Data are plotted as box-whisker plots representing the median and 95% confidence intervals (blue).

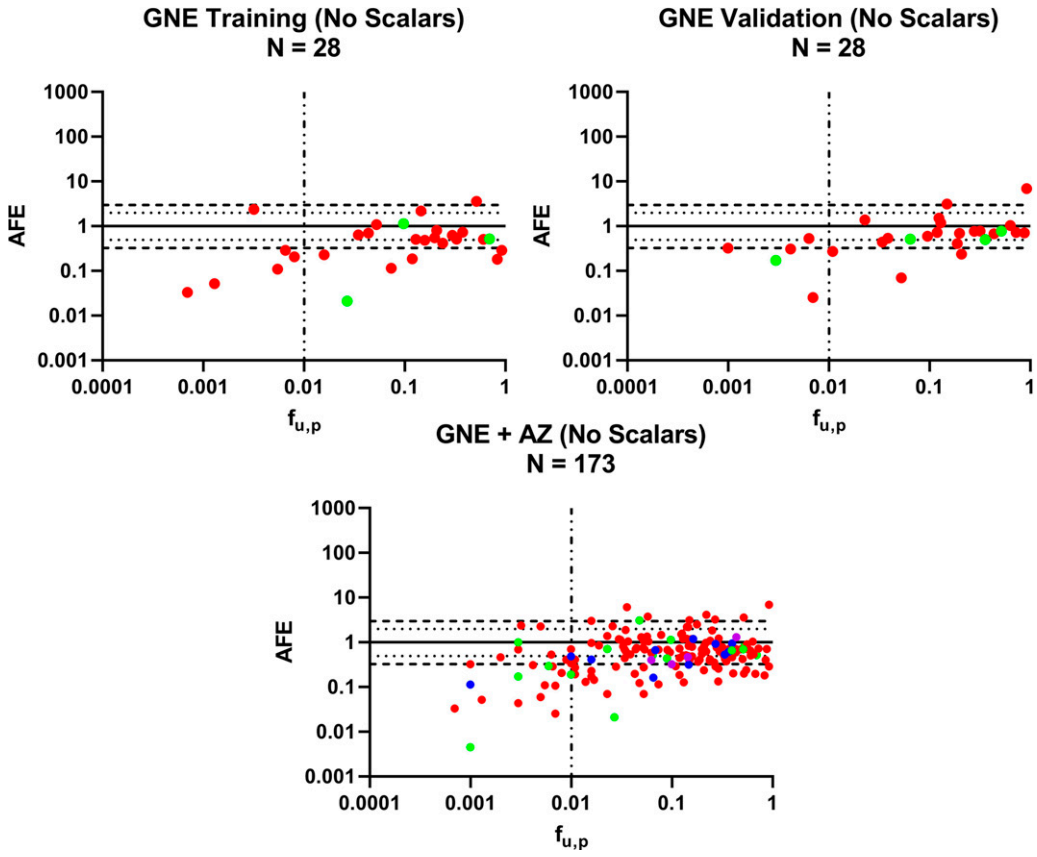

Fig. 4. Accuracy (AFE) of human clearance prediction using the well-stirred model vs. $f_{u,p}$ using no scalars (essentially, α and β both = 1). The dashed vertical line differentiates the highly bound compounds ($f_{u,p} \leq 0.01$) from the non–highly bound compounds ($f_{u,p} > 0.01$). The horizontal dashed, dotted, and solid lines represent the 3-fold error, 2-fold error, and line of unity, respectively. Compounds are color coded based on mechanism of elimination (red: CYP450 metabolism; green: phase II metabolism; blue: other; purple: unknown).

fixed to 1 and β was fitted using GNE training dataset, a β value of 0.55 was determined. Figure 6 demonstrates changes in prediction accuracy for the GNE and AZ datasets. Similar to the α scalar, as expected the CL_{pred} values were increased compared with the model predictions using no scalars due to the product of $CL_{int,u} \cdot f_{u,p}^{\beta}$, where $f_{u,p} < 1$, which improved the prediction for a majority of the compounds that were originally underpredicted. The percentage of compounds that were less than 2-fold AAFE CL_{pred} values for the GNE training, GNE validation, and GNE + AZ datasets were also reduced compared with the model prediction with no scalars (60.7%, 75.0%, and 64.7%, respectively) (Table 1). Comparing method 1 to method 2, it is apparent that the CL_{pred} values for the highly bound compounds were improved for all three datasets when using the exponential β scalar in contrast to the coefficient α scalar. Additionally, the β scalar derived using this fitting approach can also be mathematically rearranged to yield a plasma protein binding-dependent $CL_{int,u}$ scaling factor equivalent to $f_{u,p}^{\beta-1} \cdot (CL_{int,u} \cdot f_{u,p})$. Where $\beta = 0.55$ using method 2, this scaling factor simplifies to $f_{u,p}^{-0.45}$, which produced changes in CL_{pred} within 2-fold of the scaling factor derived by Francis et al. (2021) in the range of $f_{u,p}$ 0–0.0001 (Supplemental Fig. 3).

For method 3, when α and β are fit simultaneously to correct for prediction error the overall predictions do not substantially improve Fig. 7 compared with methods 1 and 2. Using this simultaneously fitting method, an α value of 1.74 and a β value of 0.66 were obtained in GNE training dataset. The percentage of compounds that were less than 2-fold AAFE CL_{pred} values for the GNE training, GNE validation, and GNE + AZ datasets were 60.7%, 75.0%, and 64.2%, respectively. Figure 8 summarizes the AAFE values across all of the scaling methods implemented in this analysis.

TABLE 1

In vitro to in vivo human CL prediction accuracy (AAFE) for different scaling methods applied to the well-stirred model, percentages of dataset where predicted CL was < or >2-fold of observed clearance, and calculated coefficients of determination (R^2)

Dataset	Accuracy	No Scalars (α = 1, β = 1)	Method 1 (α = 3.66, β = 1)	Method 2 (α = 1, β = 0.55)	Method 3 (α = 1.74, β = 0.66)
GNE training (N = 28)	<2-fold (%)	32.1	60.7	60.7	60.7
	>2-fold (%)	67.9	39.3	39.3	39.3
	AAFE	3.35	2.20	2.02	1.98
	R^2	0.70	0.74	0.64	0.69
GNE validation (N = 28)	<2-fold (%)	53.6	71.4	75.0	75.0
	>2-fold (%)	46.4	28.6	25.0	25.0
	AAFE	2.44	1.94	1.82	1.88
	R^2	0.63	0.60	0.66	0.68
GNE + AZ (N = 173)	<2-fold (%)	45.7	63.6	64.7	64.2
	>2-fold (%)	54.3	36.4	35.3	35.8
	AAFE	2.54	1.95	1.96	1.94
	R^2	0.40	0.46	0.33	0.39

TABLE 2

In vitro to in vivo human CL prediction accuracy (AAFE) for different scalar methods applied to the well-stirred model stratified by binding class

Dataset	Binding Class	*N*	No Scalars ($\alpha = 1$, $\beta = 1$)	Method 1 ($\alpha = 3.66$, $\beta = 1$)	Method 2 ($\alpha = 1$, $\beta = 0.55$)	Method 3 ($\alpha = 1.74$, $\beta = 0.66$)
GNE training ($N = 28$)	All	28	3.35	2.20	2.02	1.98
	$f_{u,p} \leq 0.01$	6	7.86	3.42	2.01	2.13
	$f_{u,p} > 0.01$	22	2.65	1.95	2.03	1.94
GNE validation ($N = 28$)	All	28	2.44	1.94	1.82	1.88
	$f_{u,p} \leq 0.01$	5	5.48	2.07	1.85	1.82
	$f_{u,p} > 0.01$	23	2.05	1.91	1.81	1.90
GNE + AZ ($N = 173$)	All	173	2.54	1.95	1.96	1.94
	$f_{u,p} \leq 0.01$	26	5.63	2.71	2.41	2.44
	$f_{u,p} > 0.01$	147	2.21	1.84	1.89	1.86

Discussion

The utilization of mechanistic or empirical scalars for the prediction of in vivo hepatic clearance from in vitro data are well established and are still being perfected with a variety of methods aimed at improving predictions using the WSM (Grime and Riley, 2006; Berezhkovskiy, 2011; Ring et al., 2011; Hallifax and Houston, 2012). The "holy grail" of the field's collective efforts has been to gain a mechanistic understanding of the observed IVIVE disconnects (typically an underestimation of in vivo clearance) and a prospective approach of predicting both preclinical and human clearance with accuracy and precision. With an eye on this goal, yet pragmatism in mind to drive drug discovery, we present an empirical approach deriving two scalars for the WSM. The first scalar, "α," is a coefficient CL_{int} scalar, which may be rationalized as accounting for loss of activity in the in vitro system relative to in vivo and/or as accounting for miscalculation of the physiologic scalar values used to translate in vitro half-life ($t_{1/2}$) to apparent CL_{int}. The second scaler, "β," for $f_{u,p}$ may be rationalized as accounting for hepatic uptake mediated by plasma proteins not present in vitro and/or inaccuracies in the determination of accurate free fraction in vitro.

Recent research suggests that larger in vitro-in vivo disconnects may be observed for compounds that are highly bound to albumin (Poulin and Haddad, 2015; Bowman et al., 2019; Kim et al., 2019; Francis et al., 2021). Attempts have been made to mechanistically account for these disconnects to improve clearance prediction accuracy. For example, the ability of plasma protein, particularly albumin, to enhance the uptake of highly bound compounds or organic anion transporting polypeptide (OATP) transporter substrates has been debated among researchers (often termed albumin-facilitated uptake) (Bowman et al., 2019, 2020, 2021; Chang et al., 2019; Kim et al., 2019; Liang et al., 2020; Bi et al., 2021). Da-Silva et al. (2018) evaluated the impact of scaling three different in vitro hepatocyte-based assays (i.e., suspension, plated, and micropatterned coculture), correcting for unbound fraction as well as adjusted $f_{u,p}$ ($f_{u,p,adjusted}$) to account for the presence of albumin-facilitated uptake phenomenon. In this case, the $f_{u,p,adjusted}$ equation

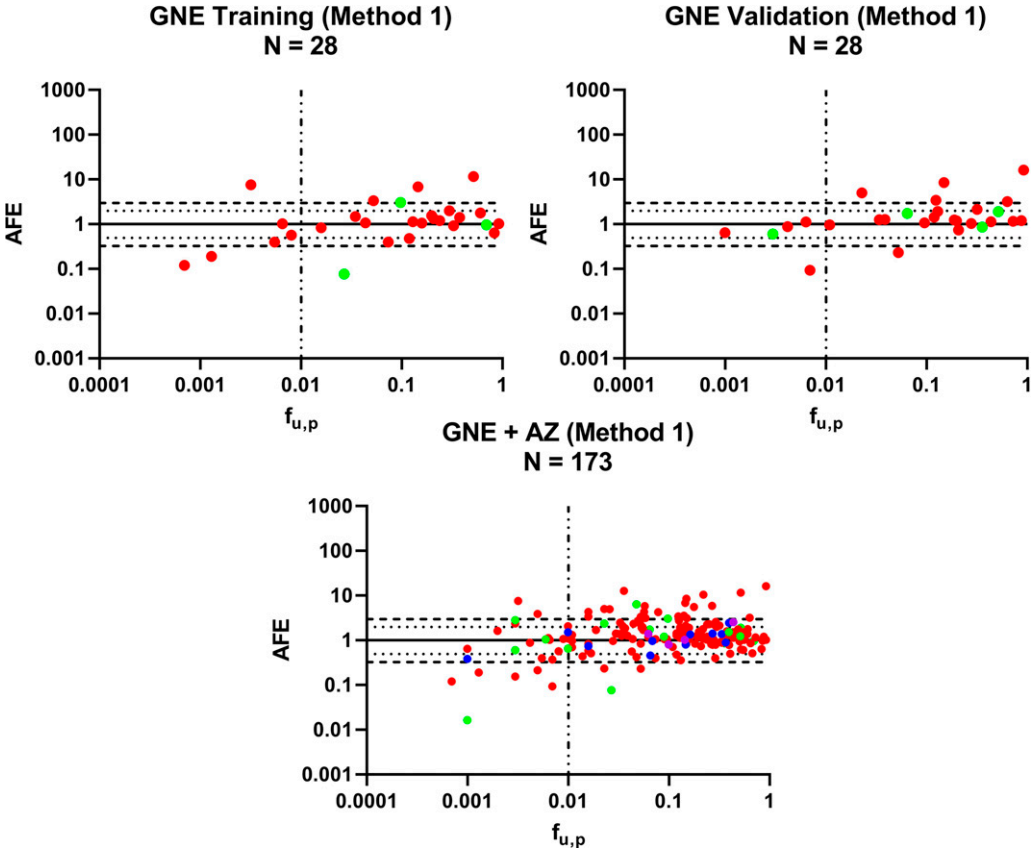

Fig. 5. Accuracy (AFE) of human clearance prediction using the well-stirred model vs. $f_{u,p}$ using method 1 ($\alpha = 3.66$, $\beta = 1$). The dashed vertical line differentiates the highly bound compounds ($f_{u,p} \leq 0.01$) from the non–highly bound compounds ($f_{u,p} > 0.01$). The horizontal dashed, dotted, and solid lines represent the 3-fold error, 2-fold error, and line of unity, respectively. Compounds are color coded based on mechanism of elimination (red: CYP450 metabolism; green: phase II metabolism; blue: other; purple: unknown).

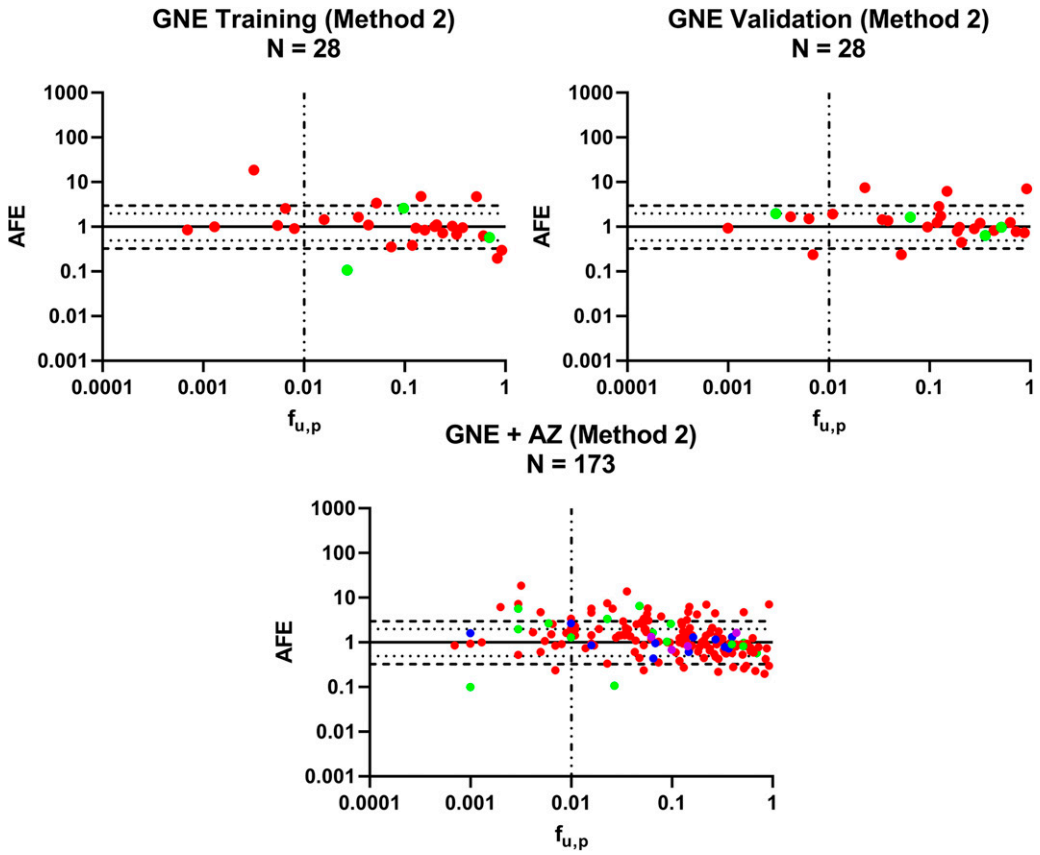

Fig. 6. Accuracy (AFE) of human clearance prediction using the well-stirred model vs. $f_{u,p}$ using method 2 ($\alpha = 1$, $\beta = 0.55$). The dashed vertical line differentiates the highly bound compounds ($f_{u,p} \leq 0.01$) from the non–highly bound compounds ($f_{u,p} > 0.01$). The horizontal dashed, dotted, and solid lines represent the 3-fold error, 2-fold error, and line of unity, respectively. Compounds are color coded based on mechanism of elimination (red: CYP450 metabolism; green: phase II metabolism; blue: other; purple: unknown).

aims to correct the experimentally determined $f_{u,p}$ values for drugs to account for the uptake of drug in cells for both bound and unbound forms based on albumin-facilitated uptake and pH gradient effect (Poulin and Haddad, 2015). Using this method, the uptake rate as a function of plasma protein binding was able to dramatically improve prediction accuracy compared with conventional $f_{u,p}$-corrected predictions (AAFE of 1.4 vs. 7.4) for a small number of compounds. These corrections increase the $f_{u,p,adjusted}$ values in comparison with original $f_{u,p}$ values,

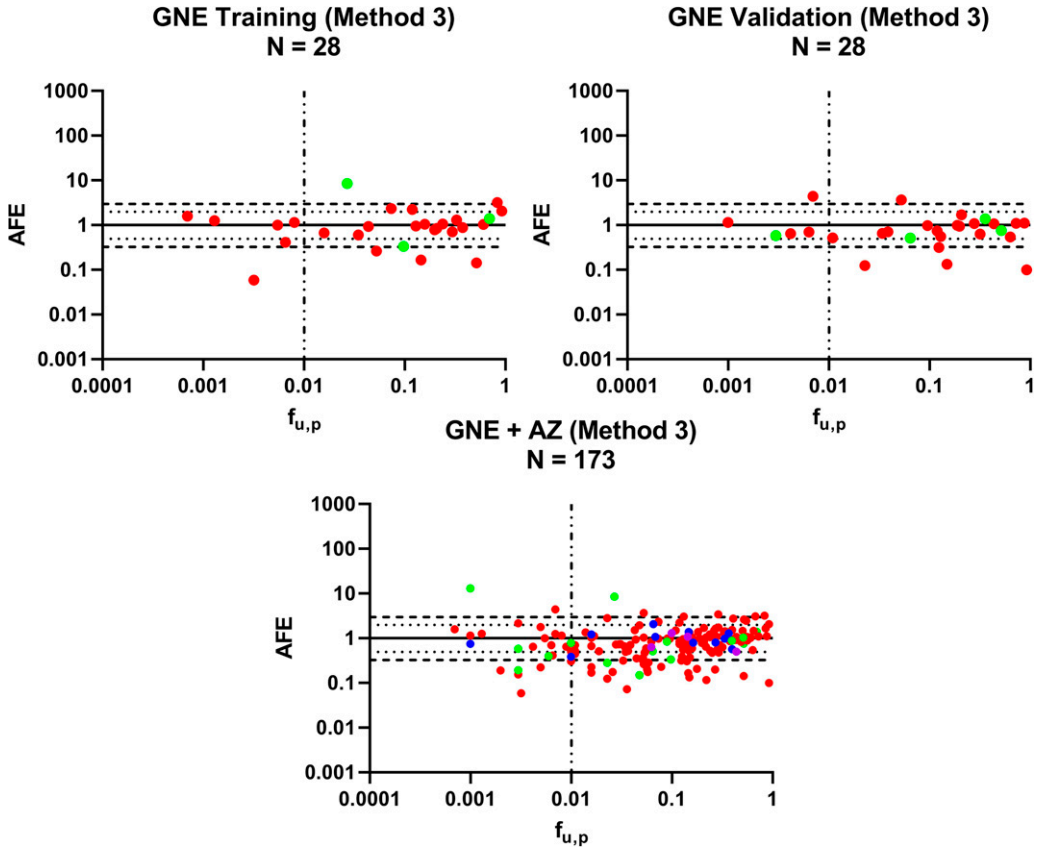

Fig. 7. Accuracy (AFE) of human clearance prediction using the well-stirred model vs. $f_{u,p}$ using method 3 ($\alpha = 1.74$, $\beta = 0.66$). The dashed vertical line differentiates the highly bound compounds ($f_{u,p} \leq 0.01$) from the non–highly bound compounds ($f_{u,p} > 0.01$). The horizontal dashed, dotted, and solid lines represent the 3-fold error, 2-fold error, and line of unity, respectively. Compounds are color coded based on mechanism of elimination (red: CYP450 metabolism; green: phase II metabolism; blue: other; purple: unknown).

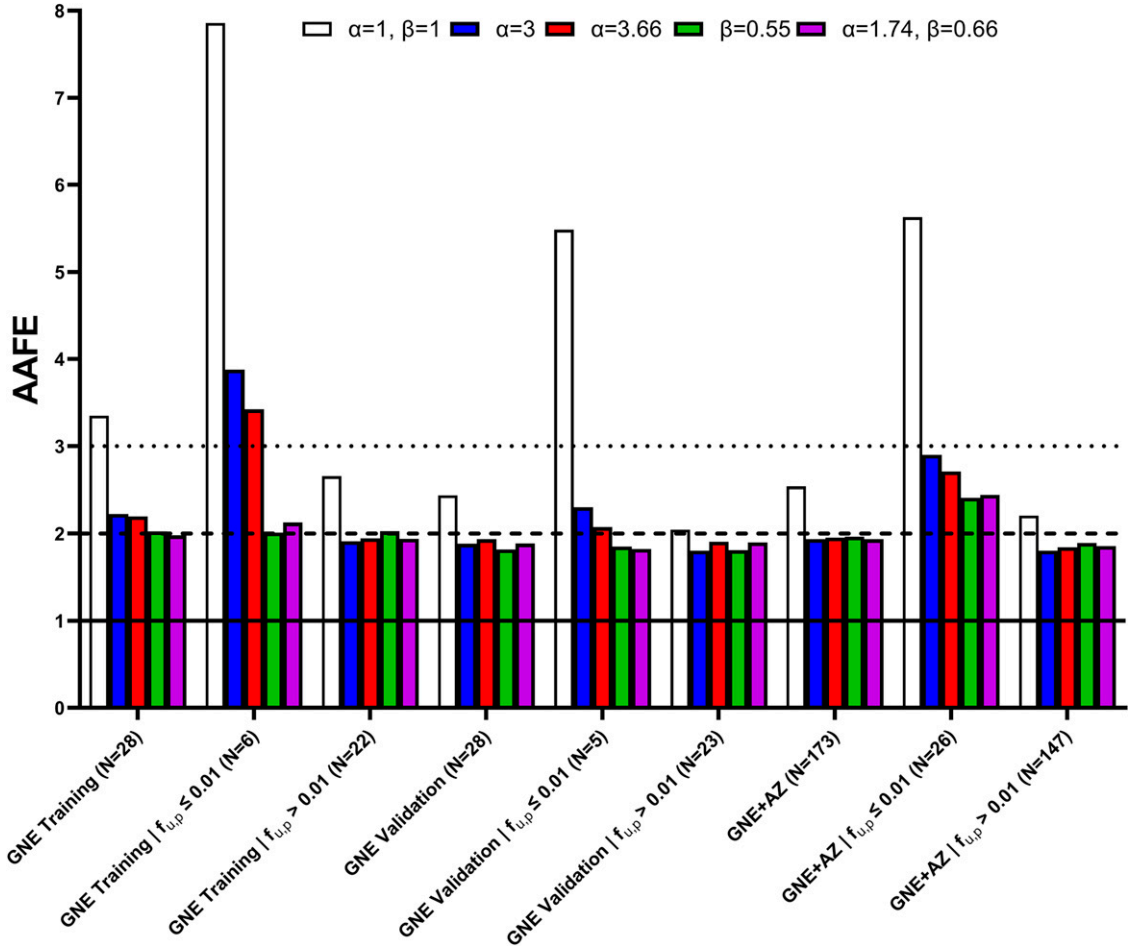

Fig. 8. Comparative summary of AAFE values across all of the scaling methods.

which are not linearly proportional to binding isotherms. The empirical scalars derived in this study are meant to address systematic underpredictions typically observed when applying the WSM. Because these scalars do not directly account for transporter activity, additional corrections might be needed for compounds for which hepatic uptake is promoted or impaired due to transporter activity. However, in recognizing the dominance of $f_{u,p}$ on CL prediction accuracy, in this current work we take a simplified approach and incorporate an exponential β scalar meant to adjust $CL_{int,u}$ values in a mechanism-agnostic fashion and independent of ionization state (differentiating from the reported $f_{u,p,adjusted}$ scaling approach). In addition to the advancement in CL IVIVE discussed, Supplemental Fig. 1 highlights how in vitro data ($CL_{int,u}$ and measured lipophilicity $\log_{D,pH=7.4}$) can also be used to diagnose the route of elimination with almost no exception outside of the −0.5–1 interval, in agreement with previous findings (Benet et al., 2011).

It is evident that all of the methods explored in this study significantly improve prediction accuracy compared with using the WSM without any scalars. The differentiation between the three methods is harder to gauge due to the relatively low number of highly bound compounds for which human intravenous clearance data are available. Although the incorporation of scalars dependent on the magnitude of plasma protein binding appears promising, the available dataset is not sufficient to draw definitive conclusions about the superiority of one method over the others.

To highlight one outlier, mifepristone ($f_{u,p}$ = 0.0032) was predicted to be within 3-fold of the CL_{obs} when not accounting for any scalars (AFE: ∼2.3); when applying methods 1–3, mifepristone CL was substantially overpredicted (method 1 using α-scalar AFE: ∼7.4; method 2 AFE: ∼18.2) and underpredicted (method 3 AFE: ∼0.06). Mifepristone is metabolized by CYP3A and has been shown to be a mechanism-based inhibitor of CYP3A4 but not CYP3A5 (Khan et al., 2002). In addition, its PK in humans is dependent on AAG binding, which limits its tissue availability (Heikinheimo et al., 2003). This observation may suggest that additional attention is required when interpreting in vitro/in vivo data for potent inhibitors of CYP3A and that caution is needed when applying a β scalar to compounds for which albumin is not the only major binding protein in plasma.

Another highly bound compound, edaravone ($f_{u,p}$ = 0.001), was poorly predicted in all cases (no scalar AFE: ∼0.004; method 1 AFE: ∼0.016; method 2 AFE: ∼0.097; method 3 AFE: ∼12.6). Despite our best efforts to only include compounds that can be adequately modeled with in vitro hepatocyte data, it is evident that this compound is known to be primarily eliminated via phase II metabolic pathways, including multiple renal/hepatic UDP-glucuronosyltransferases (UGTs) and to a lesser extent cytosolic sulfotransferases (SULTs) (FDA label: https://www.accessdata.fda.gov/drugsatfda_docs/label/2017/209176lbl.pdf). These complexities may explain disconnects observed for edaravone as well for other compounds in the dataset that can be difficult to anticipate during early phases of drug discovery.

In this work, all drugs were treated in a similar fashion independent of physiochemical properties. This is advantageous in early drug discovery where there may be several hundreds of compounds screened per therapeutic target with only limited data available. An apparent

drawback to using this approach retrospectively is the lack of identifiability in any phenomena that are particularly responsible for inaccuracies in predictions, making it nonmechanistic in nature. In cases where these scalars are applied, one could imagine the α scalar on $CL_{int,u}$ could be responsible for correcting for loss of hepatocyte activity over time, especially for low extraction drugs. In addition, because many highly bound drugs are anionic in nature and organic anion transporting polypeptide (OATP) substrates, the β scalar is amenable for accounting for any unidentifiable phenomenon (including potentially albumin-facilitated uptake). Although it is apparent that the training set of compounds used in this study (GNE training, $N = 28$) had a much lower accuracy in terms of CL predictions compared with the GNE validation and GNE + AZ datasets, based on the relative magnitude of improvement for each individual dataset using each method, the utility of these scaling approaches for improving CL predictions is evident. The application of the scalars identified in this study to a dataset of 348 compounds in preclinical species (mouse, rat, dog, and cynomolgus monkey) (data not shown) appears to support the findings observed in the human dataset: AAFE from 4.3 (no scalars) to 2.4 (method 1), 2.1 (method 2), and 2.0 (method 3). Analogous to the human dataset, the gap in accuracy between method 1 and the other two methods corresponds to a marked increase in average error observed when predicting the 29 highly bound compounds available in this set: 4.6 (method 1), 2.1 (method 2), and 2.8 (method 3). Because the scalars used in the preclinical species are derived from humans, these preliminary results suggest that they address phenomena that are species independent in their nature, also supported by previous findings using rat and human hepatocytes (Francis et al., 2021). Although more work will be necessary to mechanistically understand the reasons why these scalars appear to improve accuracy in CL predictions across different drug classes, these observations have diagnostic value and may assist additional future investigations.

Acknowledgments

The authors would like to thank Simon Wong for reviewing and providing feedback to the manuscript.

Authorship Contributions

Participated in research design: Jones, Chang, Broccatelli.

Conducted experiments: Leung, Brown, Liu.

Contributed new reagents or analytic tools: Jones, Chang, Broccatelli.

Performed data analysis: Jones, Leung, Chang, Brown, Liu, Yan, Kenny, Broccatelli.

Wrote or contributed to the writing of the manuscript: Jones, Leung, Chang, Yan, Kenny, Broccatelli.

References

Benet LZ, Broccatelli F, and Oprea TI (2011) BDDCS applied to over 900 drugs. *AAPS J* **13**:519–547.

Benet LZ and Sodhi JK (2020) Investigating the theoretical basis for in vitro-in vivo extrapolation (IVIVE) in predicting drug metabolic clearance and proposing future experimental pathways. *AAPS J* **22**:120.

Berezhkovskiy LM (2011) The corrected traditional equations for calculation of hepatic clearance that account for the difference in drug ionization in extracellular and intracellular tissue water and the corresponding corrected PBPK equation. *J Pharm Sci* **100**:1167–1183.

Bi Y-A, Ryu S, Tess DA, Rodrigues AD, and Varma MVS (2021) Effect of human plasma on hepatic uptake of organic anion-transporting polypeptide 1B substrates: studies using transfected cells and primary human hepatocytes. *Drug Metab Dispos* **49**:72–83.

Bowman CM and Benet LZ (2019) In vitro-in vivo extrapolation and hepatic clearance-dependent underprediction. *J Pharm Sci* **108**:2500–2504.

Bowman CM, Chen B, Cheong J, Liu L, Chen Y, and Mao J (2021) Improving the translation of organic anion transporting polypeptide substrates using HEK293 cell data in the presence and absence of human plasma via PBPK modeling. *Drug Metab Dispos* **49**:530–539.

Bowman CM, Chen E, Chen L, Chen Y-C, Liang X, Wright M, Chen Y, and Mao J (2020) Changes in organic anion transporting polypeptide uptake in HEK293 overexpressing cells in the presence and absence of human plasma. *Drug Metab Dispos* **48**:18–24.

Bowman CM, Okochi H, and Benet LZ (2019) The presence of a transporter-induced protein binding shift: a new explanation for protein-facilitated uptake and improvement for in vitro-in vivo extrapolation. *Drug Metab Dispos* **47**:358–363.

Chang JH, Chen Y-C, Cheong J, Jones RS, and Pang J (2019) Investigating the impact of albumin on the liver uptake of pitavastatin and warfarin in Nagase analbuminemic rats. *Drug Metab Dispos* **47**:1307–1313.

Chen S, Garcia LP, Bergström FH, Nordell P, and Grime K (2017) Intrinsic clearance assay incubational binding: a method comparison. *Drug Metab Dispos* **45**:342–345.

Da-Silva F, Boulenc X, Vermet H, Compigne P, Gerbal-Chaloin S, Daujat-Chavanieu M, Klieber S, and Poulin P (2018) Improving prediction of metabolic clearance using quantitative extrapolation of results obtained from human hepatic micropatterned cocultures model and by considering the impact of albumin binding. *J Pharm Sci* **107**:1957–1972.

Endres CJ, Endres MG, and Unadkat JD (2009) Interplay of drug metabolism and transport: a real phenomenon or an artifact of the site of measurement? *Mol Pharm* **6**:1756–1765.

Francis LJ, Houston B, and Hallifax D (2021) Impact of plasma protein binding in drug clearance prediction: a database analysis of published studies and implications for in vitro in vivo extrapolation. *Drug Metab Dispos* **49**:188–201.

Gammans RE, Mayol RF, and LaBudde JA (1986) Metabolism and disposition of buspirone. *Am J Med* **80** (3B):41–51.

Grime K and Riley RJ (2006) The impact of in vitro binding on in vitro-in vivo extrapolations, projections of metabolic clearance and clinical drug-drug interactions. *Curr Drug Metab* **7**:251–264.

Hallifax D, Foster JA, and Houston JB (2010) Prediction of human metabolic clearance from in vitro systems: retrospective analysis and prospective view. *Pharm Res* **27**:2150–2161.

Hallifax D and Houston JB (2012) Evaluation of hepatic clearance prediction using in vitro data: emphasis on fraction unbound in plasma and drug ionisation using a database of 107 drugs. *J Pharm Sci* **101**:2645–2652.

He H, Tran P, Yin H, Smith H, Batard Y, Wang L, Einolf H, Gu H, Mangold JB, Fischer V, et al. (2009) Absorption, metabolism, and excretion of [14C]vildagliptin, a novel dipeptidyl peptidase 4 inhibitor, in humans. *Drug Metab Dispos* **37**:536–544.

Heikinheimo O, Kekkonen R, and Lähteenmäki P (2003) The pharmacokinetics of mifepristone in humans reveal insights into differential mechanisms of antiprogestin action. *Contraception* **68**:421–426.

Jornil J, Jensen KG, Larsen F, and Linnet K (2010) Identification of cytochrome P450 isoforms involved in the metabolism of paroxetine and estimation of their importance for human paroxetine metabolism using a population-based simulator. *Drug Metab Dispos* **38**:376–385.

Khan KK, He YQ, Correia MA, and Halpert JR (2002) Differential oxidation of mifepristone by cytochromes P450 3A4 and 3A5: selective inactivation of P450 3A4. *Drug Metab Dispos* **30**:985–990.

Kim S-J, Lee K-R, Miyauchi S, and Sugiyama Y (2019) Extrapolation of in vivo hepatic clearance from in vitro uptake clearance by suspended human hepatocytes (IVIVE) for anionic drugs with high binding to human albumin: improvement of IVIVE by considering the "albumin-mediated" hepatic uptake mechanism based on the facilitated-dissociation model. *Drug Metab Dispos* **47**:94–103.

Kogame A, Lee R, Pan L, Sudo M, Nonaka M, Moriya Y, Higuchi T, and Tagawa Y (2019) Disposition and metabolism of the G protein-coupled receptor 40 agonist TAK-875 (fasiglifam) in rats, dogs, and humans. *Xenobiotica* **49**:433–445.

Laurenzana EM and Owens SM (1997) Metabolism of phencyclidine by human liver microsomes. *Drug Metab Dispos* **25**:557–563.

Li X-Q, Björkman A, Andersson TB, Ridderström M, and Masimirembwa CM (2002) Amodiaquine clearance and its metabolism to N-desethylamodiaquine is mediated by CYP2C8: a new high affinity and turnover enzyme-specific probe substrate. *J Pharmacol Exp Ther* **300**:399–407.

Liang X, Park Y, DeForest N, Hao J, Zhao X, Niu C, Wang K, Smith BJ, and Lai Y (2020) In vitro hepatic uptake in human and monkey hepatocytes in the presence and absence of serum protein and its in vitro to in vivo extrapolation. *Drug Metab Dispos* **48**:1283–1292.

Lombardo F, Berellini G, and Obach RS (2018) Trend analysis of a database of intravenous pharmacokinetic parameters in humans for 1352 drug compounds. *Drug Metab Dispos* **46**:1466–1477.

Lombardo F, Obach RS, Varma MV, Stringer R, and Berellini G (2014) Clearance mechanism assignment and total clearance prediction in human based upon in silico models. *J Med Chem* **57**:4397–4405.

MacLauchlin C, Schneider SE, Keedy K, Fernandes P, and Jamieson BD (2018) Metabolism, excretion, and mass balance of solithromycin in humans. *Antimicrob Agents Chemother* **62**:e01474–e17.

Madden S, Spaldin V, and Park BK (1995) Clinical pharmacokinetics of tacrine. *Clin Pharmacokinet* **28**:449–457.

McDonald MG and Rettie AE (2007) Sequential metabolism and bioactivation of the hepatotoxin benzbromarone: formation of glutathione adducts from a catechol intermediate. *Chem Res Toxicol* **20**:1833–1842.

Moise PA, Birmingham MC, and Schentag JJ (2000) Pharmacokinetics and metabolism of moxifloxacin. *Drugs Today (Barc)* **36**:229–244.

Moridani MY, Khan S, Chan T, Teng S, Beard K, and O'Brien PJ (2001) Cytochrome P450 2E1 metabolically activates propargyl alcohol: propiolaldehyde-induced hepatocyte cytotoxicity. *Chem Biol Interact* **130–132**:931–942.

Olkkola KT and Ahonen J (2008) Midazolam and other benzodiazepines. *Handb Exp Pharmacol* **182**:335–360.

Pang KS, Han YR, Noh K, Lee PI, and Rowland M (2019) Hepatic clearance concepts and misconceptions: why the well-stirred model is still used even though it is not physiologic reality? *Biochem Pharmacol* **169**:113596.

Pang KS and Rowland M (1977a) Hepatic clearance of drugs. II. Experimental evidence for acceptance of the "well-stirred" model over the "parallel tube" model using lidocaine in the perfused rat liver in situ preparation. *J Pharmacokinet Biopharm* **5**:655–680.

Pang KS and Rowland M (1977b) Hepatic clearance of drugs. I. Theoretical considerations of a "well-stirred" model and a "parallel tube" model. Influence of hepatic blood flow, plasma and blood cell binding, and the hepatocellular enzymatic activity on hepatic drug clearance. *J Pharmacokinet Biopharm* **5**:625–653.

Poulin P and Haddad S (2015) Albumin and uptake of drugs in cells: additional validation exercises of a recently published equation that quantifies the albumin-facilitated uptake mechanism(s) in physiologically based pharmacokinetic and pharmacodynamic modeling research. *J Pharm Sci* **104**:4448–4458.

Poulin P and Haddad S (2021) A new guidance for the prediction of hepatic clearance in the early drug discovery and development from the in vitro-to-in vivo extrapolation method and an approach for exploring whether an albumin-mediated hepatic uptake phenomenon could be present under in vivo conditions. *J Pharm Sci* **110**:2841–2858.

Ring BJ, Chien JY, Adkison KK, Jones HM, Rowland M, Jones RD, Yates JWT, Ku MS, Gibson CR, He H, et al. (2011) PhRMA CPCDC initiative on predictive models of human pharmacokinetics, part 3: comparative assessment of prediction methods of human clearance. *J Pharm Sci* **100**:4090–4110.

Salerno SN, Edginton A, Cohen-Wolkowiez M, Hornik CP, Watt KM, Jamieson BD, and Gonzalez D (2017) Development of an adult physiologically based pharmacokinetic model of solithromycin in plasma and epithelial lining fluid. *CPT Pharmacometrics Syst Pharmacol* **6**:814–822.

Shet MS, McPhaul M, Fisher CW, Stallings NR, and Estabrook RW (1997) Metabolism of the antiandrogenic drug (Flutamide) by human CYP1A2. *Drug Metab Dispos* **25**: 1298–1303.

Umehara K, Cantrill C, Wittwer MB, Lenarda ED, Klammers F, Ekiciler A, Parrott N, Fowler S, and Ullah M (2020) Application of the extended clearance classification system (ECCS) in drug discovery and development: selection of appropriate in vitro tools and clearance prediction. *Drug Metab Dispos* **48**:849–860.

Varma MV, Steyn SJ, Allerton C, and El-Kattan AF (2015) Predicting clearance mechanism in drug discovery: extended clearance classification system (ECCS). *Pharm Res* **32**:3785–3802.

Williamson B, Harlfinger S, and McGinnity DF (2020) Evaluation of the disconnect between hepatocyte and microsome intrinsic clearance and in vitro in vivo extrapolation performance. *Drug Metab Dispos* **48**:1137–1146.

Winiwarter S, Chang G, Desai P, Menzel K, Faller B, Arimoto R, Keefer C, and Broccatell F (2019) Prediction of fraction unbound in microsomal and hepatocyte incubations: a comparison of methods across industry datasets. *Mol Pharm* **16**:4077–4085.

Yu K, Geng X, Chen M, Zhang J, Wang B, Ilic K, and Tong W (2014) High daily dose and being a substrate of cytochrome P450 enzymes are two important predictors of drug-induced liver injury. *Drug Metab Dispos* **42**:744–750.

Address correspondence to: Dr. Fabio Broccatelli, Drug Metabolism and Pharmacokinetics, Genentech, Inc., 1 DNA Way, South San Francisco, CA 94080. E-mail: fabio.broccatelli@gmail.com

Supplemental Information

Application of empirical scalars to enable early prediction of human hepatic clearance using IVIVE in drug discovery: an evaluation of 173 drugs

Authors: Robert S. Jones[1], Christian Leung[1], Jae H. Chang[2], Suzanne Brown[3], Ning Liu[4], Zhengyin Yan[1], Jane R. Kenny[1], Fabio Broccatelli[1]

[1] Drug Metabolism and Pharmacokinetics, Genentech, Inc., South San Francisco, CA, 94080

[2] Exelixis, Drug Discovery Sciences, Alameda, CA 94502

[3] Ultragenyx Pharmaceutical Inc., Novato, CA 94949

[4]Avirmax, Inc., Hayward, CA 94541

Journal: Drug Metabolism and Disposition

Manuscript ID: DMD-AR-2021-000784

Supplemental Table 1: GNE compound list and in vitro parameters determined in human plasma ($f_{u,p}$), hepatocytes (CL_{int}) and microsomes ($f_{u,mic}$) used for CL predictions (N = 56). In vitro data are presented as mean values from experiments performed in triplicate.

Drug	Elimination Pathway	$f_{u,p}$	CL_{int} (mL/min/kg)	$f_{u,mic}$	$CL_{int,u}$ (mL/min/kg)	CL_{obs} (mL/min/kg)
Acetaminophen	P2	0.52	8.7	0.979	8.9	5
Ambrisentan	P2	0.027	0.4	1	0.4	0.54
Amitriptyline HCl	CYP	0.12	32	0.4	80	9.34
Antipyrine	CYP	0.93	5.8	1	5.8	0.64
Caffeine	CYP	0.64	2.4	1	2.4	1.4
Chlorpromazine	CYP	0.044	40	0.076	526.3	16
Citalopram	CYP	0.2	10.7	0.828	12.9	4.3
Clomipramine HCl	CYP	0.039	30.3	0.22	137.9	8.2
Clonazepam	CYP	0.15	16.1	0.79	20.4	0.88
Clozapine	P2	0.098	17	0.526	32.3	2.5
Codeine	P2	0.7	16.4	0.961	17.1	15
Cyclobenzaprine	CYP	0.13	23	0.46	50	10
Cyclophosphamide	CYP	0.93	0.3	0.977	0.3	1.1
Desipramine	CYP	0.16	17	0.394	43.1	11
Dexamethasone	CYP	0.32	7.1	0.799	8.8	3.3
Diphenhydramine	CYP	0.38	25	0.9	27.8	9.8
Dronedarone	CYP	0.001	38	0.004	9500	20.7
Gefitinib	CYP	0.053	6.1	0.38	16.1	12
Glimepiride	CYP	0.001	21.6	0.94	23	0.5
Glyburide	CYP	0.001	24	0.75	32	0.82
Ibuprofen	CYP	0.011	19	0.953	19.9	0.82
Imatinib	CYP	0.125	35	0.687	50.9	3.3
Imipramine	CYP	0.2	40.1	0.535	75	13
Indinavir	P2	0.36	28.5	0.672	42.4	18
Lidocaine	CYP	0.33	36.7	0.937	39.2	16
Meloxicam	CYP	0.007	0.4	0.942	0.4	0.12
Metoprolol	CYP	0.88	17.1	0.946	18.1	13
Midazolam	CYP	0.034	53.4	0.712	74.9	5.3
Mifepristone	CYP	0.003	80.3	0.21	382.4	0.5
Nefazodone	CYP	0.004	125	0.207	603.9	7.5
Nevirapine	CYP	0.52	2.1	1	2.1	0.3

Nicardipine	CYP	0.006	160	0.131	1221.4	11
Nifedipine	CYP	0.035	105	0.63	166.7	7.3
Olanzapine	CYP	0.21	6.4	0.96	6.7	5.7
Oxazepam	P2	0.065	6.6	0.765	8.6	1.1
Paroxetine	CYP	0.12	8	0.25	32	18
Pefloxacin	CYP	0.84	0.3	0.793	0.4	2
Pioglitazone	CYP	0.006	18.7	0.68	27.5	1.4
Promethazine	CYP	0.096	54.5	0.39	139.7	14
Propranolol	CYP	0.21	78	0.961	81.2	12
Quinacrine	CYP	0.24	6.4	0.67	9.6	5.1
Quinidine	CYP	0.19	7.5	0.832	9	4
Quinine	CYP	0.3	3.6	0.884	4.1	1.9
Rosiglitazone	CYP	0.007	21.9	0.79	27.8	0.65
Saquinavir	CYP	0.008	59	0.16	368.8	13
Sulfinpyrazone	CYP	0.016	4.2	0.877	4.8	0.34
Tamsulosin	CYP	0.146	9.1	0.94	9.7	0.62
Telithromycin	CYP	0.44	38	1	38	14
Theophylline	CYP	0.61	0.7	0.982	0.7	0.86
Tolcapone	P2	0.003	34.6	0.323	107.1	1.9
Tolterodine	CYP	0.13	100	0.71	140.8	8.4
Trazodone HCl	CYP	0.053	26.9	0.9	29.9	1.4
Venlafaxine	CYP	0.73	23.6	0.922	25.6	14
Verapamil	CYP	0.28	105.5	0.782	134.9	18
Warfarin	CYP	0.023	2.6	0.813	3.2	0.055
Zolpidem	CYP	0.074	6	0.899	6.7	4.3

Supplemental Table 2: AZ compound list and parameters used for CL predictions (N = 117) (Williamson *et al.*, 2020).

Drug	Elimination Pathway	$f_{u,p}$	$CL_{int,u}{}^{*}$ (mL/min/kg)	CL_{obs} (mL/min/kg)
Adinazolam	CYP	0.352	9.9	6.2
Alfuzosin	CYP	0.292	5.4	5.9
Alprenolol	CYP	0.150	52.9	15.0
Amsacrine	CYP	0.007	65.2	4.3
Antazoline	CYP	0.562	184.2	19.7
Axitinib	CYP	0.003	71.2	5.0
Azelastine	CYP	0.145	37.6	9.0
Basimglurant	CYP	0.010	209.5	2.8
Bendamustine	CYP	0.050	155.6	4.5
Benperidol	CYP	0.219	58.3	8.3
Bevantolol	CYP	0.127	111.4	5.5
Bortezomib	CYP	0.132	20.2	19.0
Bunazosin	CYP	0.120	19.2	4.8
Bupivacaine	CYP	0.148	28.4	4.3
Carvedilol	CYP	0.019	495.9	7.8
Cilomilast	CYP	0.011	8.6	0.5
Clarithromycin	CYP	0.350	8.8	7.3
Clindamycin	CYP	0.286	17.3	4.5
Clomipramine	CYP	0.037	379.4	8.2
Conivaptan	CYP	0.010	103.7	3.0
Cyclizine	CYP	0.339	25.0	14.5
Dabrafenib	CYP	0.011	109.9	2.9
Dexloxiglumide	CYP	0.016	39.7	3.7
Diazepam	CYP	0.016	22.7	0.4
Diltiazem	CYP	0.265	21.6	13.0
Dimetindene	CYP	0.294	26.8	4.8
Dinaciclib	CYP	0.142	136.5	4.7
Dofetilide	CYP	0.490	8.7	5.2
Domperidone	CYP	0.034	276.7	9.5
Doxazosin	CYP	0.059	29.8	1.6
Doxepin	CYP	0.221	64.4	14.0
Duloxetine	CYP	0.055	392.3	8.6
Encainide	CYP	0.572	27.0	13.0

Enoximone	CYP	0.410	11.2	19.1
Erlotinib	CYP	0.052	25.5	1.7
Erythromycin	CYP	0.353	9.0	5.6
Etonogestrel	CYP	0.033	52.0	2.0
Fimasartan	CYP	0.023	29.2	9.6
Finasteride	CYP	0.139	9.2	2.4
Flupentixol	CYP	0.016	1815.1	4.1
Fluphenazine	CYP	0.035	3479.0	9.7
Gestodene	CYP	0.057	19.3	0.8
Gisadenafil	CYP	0.552	7.2	14.3
Granisetron	CYP	0.607	13.3	9.1
Hydrocortisone	CYP	0.380	11.0	5.7
Idrocilamide	CYP	0.036	226.9	1.0
Indisulam	CYP	0.003	165.0	0.7
Ketamine	CYP	0.652	29.2	19.0
Levomepromazine	CYP	0.056	375.6	9.9
Levonorgestrel	CYP	0.045	31.0	1.8
Melatonin	CYP	0.679	5.5	16.5
Mepivacaine	CYP	0.524	2.7	6.8
Mibefradil	CYP	0.005	3039.0	4.0
Mirabegron	CYP	0.290	6.7	13.6
Mirtazapine	CYP	0.239	14.9	8.0
Nateglinide	CYP	0.017	15.1	1.8
Nebivolol	CYP	0.030	2295.9	14.0
Nefopam	CYP	0.507	12.8	12.0
Nortilidine	CYP	0.862	5.5	9.9
Ondansetron	CYP	0.435	9.2	5.8
Panobinostat	CYP	0.391	25.1	10.2
Pantoprazole	CYP	0.028	22.3	2.2
Papaverine	CYP	0.063	141.5	11.0
Paritaprevir	CYP	0.014	53.8	5.7
Pimobendan	CYP	0.110	44.6	14.0
Prazosin	CYP	0.048	12.1	4.7
Prednisone	CYP	0.270	46.9	2.5
Prochlorperazine	CYP	0.141	1341.6	16.0
Procyclidine	CYP	0.222	18.6	0.9
Promazine	CYP	0.158	442.8	14.0
Propafenone	CYP	0.074	296.3	16.0
Propiverine	CYP	0.058	387.1	2.9

Ramelteon	CYP	0.183	32.9	13.1
Ranolazine	CYP	0.435	22.1	9.5
Reboxetine	CYP	0.152	5.1	0.8
Repaglinide	CYP	0.009	403.6	7.8
Riluzole	CYP	0.043	56.0	11.3
Risperidone	CYP	0.160	32.8	5.4
Roflumilast	CYP	0.005	25.6	2.2
Ropivacaine	CYP	0.242	33.1	5.5
Semaxanib	CYP	0.031	2000.0	14.0
Solifenacin	CYP	0.179	38.2	2.1
Tasimelteon	CYP	0.274	10.5	9.0
Telcagepant	CYP	0.053	31.8	5.8
Tolamolol	CYP	0.348	28.9	14.0
Tolterodine	CYP	0.253	219.2	8.4
Tolvaptan	CYP	0.026	277.3	2.4
Trazodone	CYP	0.079	27.9	1.4
Trimipramine	CYP	0.091	235.3	16.0
Verlukast	CYP	0.002	154.6	0.7
Vilazodone	CYP	0.054	53.2	3.8
Vinorelbine	CYP	0.400	40.0	20.0
Voriconazole	CYP	0.566	15.0	8.3
Chlorambucil	OTHER	0.010	139.9	2.8
Danusertib	OTHER	0.337	10.9	6.1
Dexmedetomidine	OTHER	0.148	27.3	11.0
Mebendazole	OTHER	0.066	40.7	15.0
Metopimazine	OTHER	0.273	83.9	12.1
Nintedanib	OTHER	0.016	809.3	19.9
Remimazolam	OTHER	0.164	669.3	15.0
Selegiline	OTHER	0.369	77.5	20.0
Thalidomide	OTHER	0.400	9.2	3.4
Tozasertib	OTHER	0.069	412.0	18.4
Ziprasidone	OTHER	0.001	575.7	5.1
Canagliflozin	P2	0.010	51.9	2.7
Deferasirox	P2	0.006	40.6	0.8
Dipyridamole	P2	0.048	176.9	2.0
Edaravone	P2	0.001	6.2	1.4
Flavopiridol	P2	0.090	33.0	6.1
Irinotecan	P2	0.397	14.4	7.0
Mizolastine	P2	0.023	31.7	1.0

Olodaterol	P2	0.516	27.5	12.5
Tolfenamic acid	P2	0.003	863.9	2.4
Biperiden	UNK	0.100	46.4	12.0
Doxapram	UNK	0.440	22.4	5.3
Ridogrel	UNK	0.063	6.6	1.1
Volasertib	UNK	0.145	48.9	11.6

*Values were calculated using internal physiological scaling factors and raw data published in Supplemental Information (Williamson *et al.*, 2020).

Supplemental Figure 1: Unbound intrinsic CL ($CL_{int,u}$) versus $log_{D,pH=7.4}$ for the GNE dataset (N = 56) with 22 additional compounds, including those undergoing non-metabolic routes of elimination (total N = 78). In vitro data are mean values from experiments performed in triplicate. Data is stratified by major mechanism of elimination denoted by color (red: CYP-mediated, green: phase II metabolism, yellow: renal elimination, purple: biliary elimination).

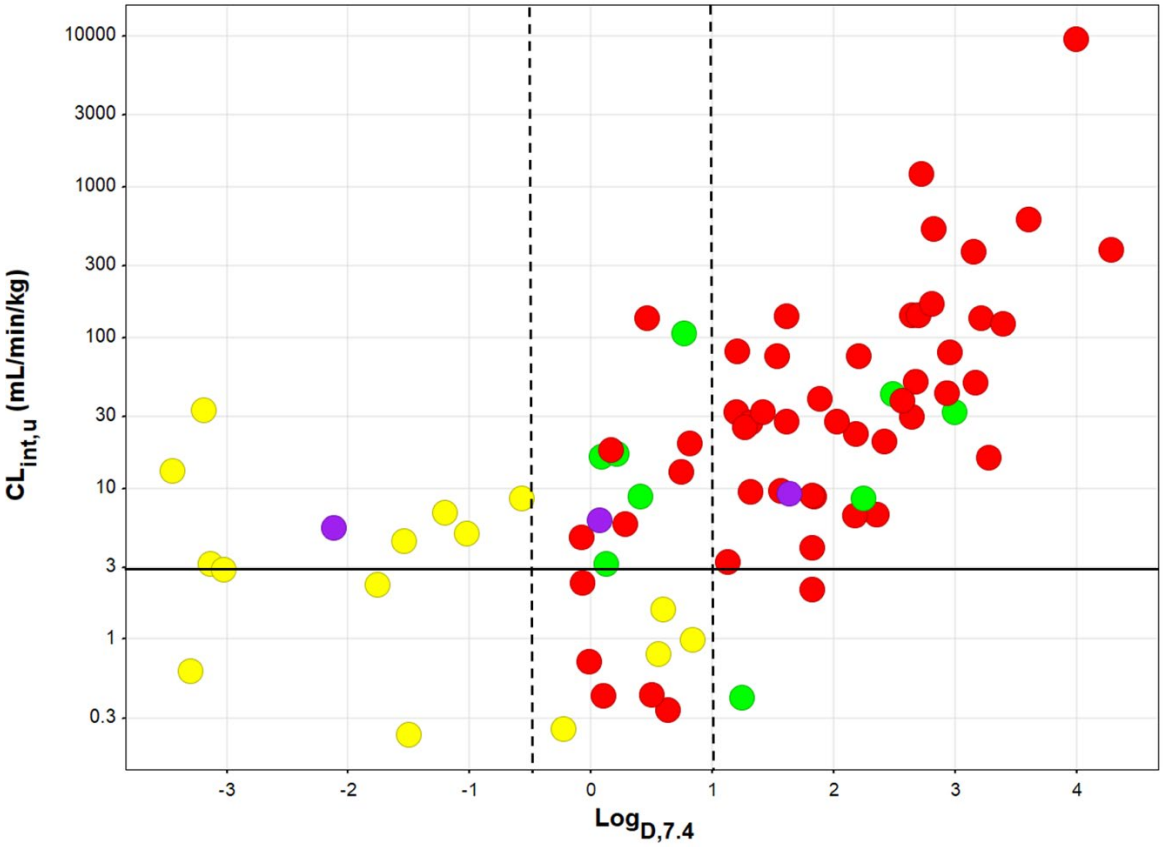

Supplemental Figure 2: Correlation plots of CL_{pred} vs. CL_{obs} of the GNE + AZ datasets for each of the scaling methods.

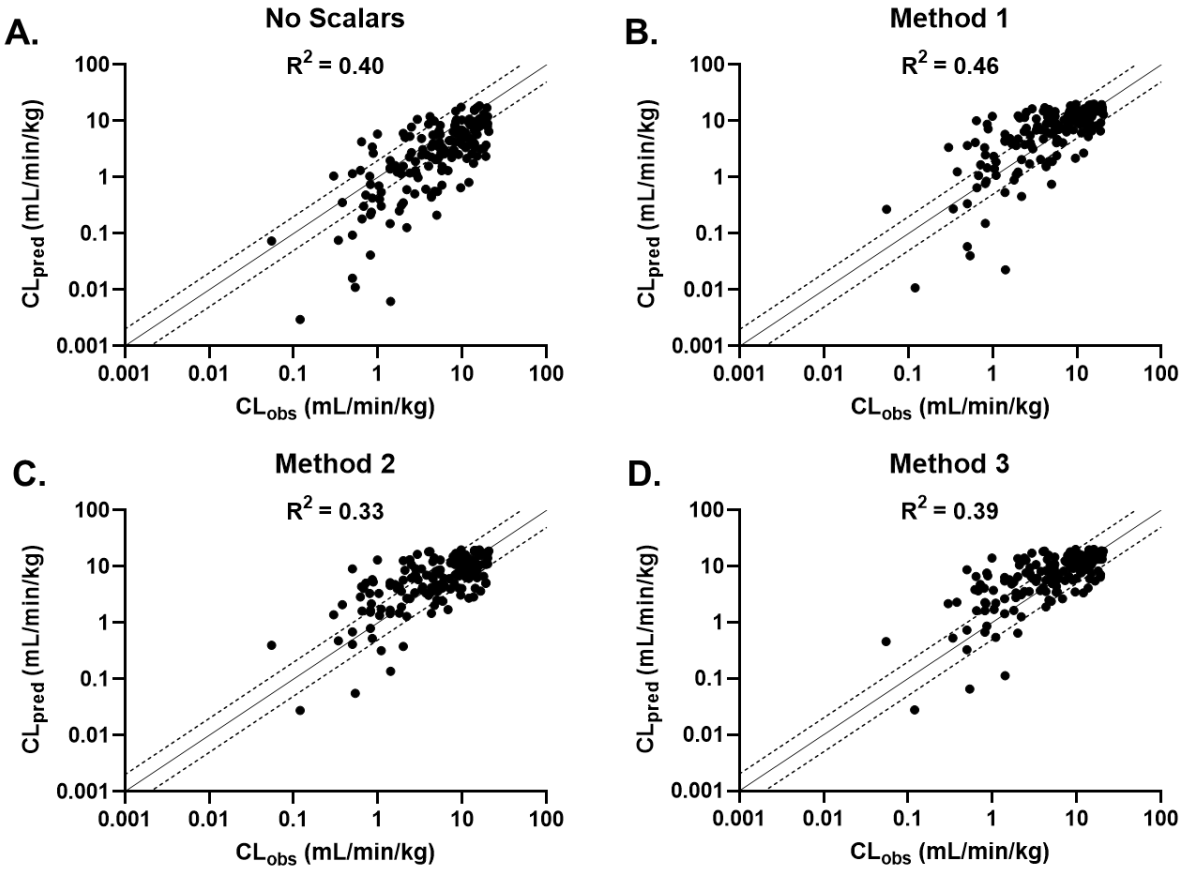

Supplemental Figure 3. A comparison in fold-change in $CL_{int,u}$ with respect to $f_{u,p}$ between two modeling approaches (Francis et al. and GNE method 2 using the β scalar). The impact of these scalars on $CL_{int,u}$ are within 2-fold of each other ($f_{u,p}$ ranging from 0.0001 – 1) (Francis *et al.*, 2020).